PHYSICAL REVIEW D **95,** 035036 (2017)

Diphoton signal of a light pseudoscalar in the NMSSM at the LHC

Monoranjan Guchait[*] and Jacky Kumar[†]

Department of High Energy Physics, Tata Institute of Fundamental Research, Homi Bhabha Road, Mumbai-400005, India

(Received 24 September 2016; published 28 February 2017)

We explore the detection possibility of the light pseudoscalar Higgs boson in the next-to-minimal supersymmetric standard model (NMSSM) at the LHC with the center of mass energy, $\sqrt{S} = 13$ TeV. We focus on the parameter space which provides one of the Higgs bosons as SM-like with a mass of 125 GeV and some of the non-SM-like Higgs bosons can be light having suppressed couplings with fermions and gauge bosons due to their singlet nature. It is observed that for a certain region of model parameter space, the singlet-like light pseudoscalar can decay to the diphoton ($\gamma\gamma$) channel with a substantial branching ratio. In this study, we consider this diphoton signal of a light pseudoscalar Higgs boson producing it through the chargino-neutralino production and the subsequent decay of the neutralino. We consider the signal consisting of two photons plus missing energy along with a lepton from the chargino decay. Performing a detailed simulation of the signal and backgrounds including detector effects, we present results for a few benchmark points corresponding to the pseudoscalar Higgs boson mass in the range 60–100 GeV. Our studies indicate that some of the benchmark points in the parameter space can be probed with a reasonable significance for 100 fb^{-1} integrated luminosity. We also conclude that exploiting this channel it is possible to distinguish the NMSSM from the other supersymmetric models.

DOI: 10.1103/PhysRevD.95.035036

I. INTRODUCTION

In spite of the absence of any signal of superpartners at the LHC, still supersymmetry (SUSY) remains one of the best possible options for the physics beyond standard model (BSM). Looking for its signal is a very high priority task in the next phase of LHC experiments. The SUSY models provide a solution for the hierarchy problem, unification of gauge couplings at a certain high energy scale and in addition, offers a dark matter candidate which is absent in the standard model (SM). In order to interpret the recently discovered Higgs particle ($H_{\rm SM}$) of mass ~125 GeV at the LHC [1,2] in the framework of the minimal supersymmetric standard model (MSSM), one requires a special kind of parameter space, in particular for the squark sector of the third generation [3,4]. For instance, the lightest Higgs boson of mass ~125 GeV in the MSSM can be obtained either by pushing up the lighter top squark mass to a larger value or assuming a maximal mixing in the top squark sector. Moreover, the μ term in the superpotential, $\mu H_u H_{\rm d}$ is a another potential source of problem, where H_u and H_d are the two Higgs doublets required to generate the up- and down-type fermion masses. The value of μ is expected to be around the electroweak (EW) scale $\sim\mathcal{O}(100\ \text{GeV})$, but nothing constrain it not to accept a large value. In fact, it can go far above the EW scale, which is known as the μ-problem [5]. In the framework of the next-to-minimal supersymmetric model (NMSSM) these issues can be addressed more naturally [6–8]. The NMSSM contains an extra Higgs singlet (S) field, in addition to the two Higgs doublets H_u, H_d like the MSSM. The superpotential reads as

$$W_{\rm NMSSM} = W_{\rm MSSM} + \lambda S H_u H_d + \frac{1}{3}\kappa S^3, \qquad (1.1)$$

where λ and κ are the dimensionless couplings and $W_{\rm MSSM}$ is identical to the superpotential in MSSM except the μ term. The vacuum expectation value (VEV) v_s of the singlet field generates the μ term dynamically, i.e. $\mu_{\rm eff} = \lambda v_s$. The Higgs sector of the NMSSM contains three neutral CP-even (H_1, H_2, H_3; $m_{H_1} < m_{H_2} < m_{H_3}$) and two CP-odd neutral pseudoscalars (A_1, A_2; $m_{A_1} < m_{A_2}$) plus charged Higgs boson ($H^{\pm}$) states (for details, see the review of Refs. [9,10]). The states of the physical neutral Higgs bosons are composed of both the singlet and the doublet fields. Interestingly, one of the CP-even neutral Higgs bosons can be interpreted as the recently found SM-like Higgs boson and it remains valid for a wide range of model parameters [11–16] and, unlike the MSSM, it does not require much fine-tuning of the model parameters. It can be attributed to the mixing of the singlet Higgs field with the doublets via the $\lambda S H_u H_d$ term. This interaction in turn lifts the tree level Higgs boson mass substantially and further contributions due to the radiative correction enable one to achieve the required Higgs boson mass of ~125 GeV [15,16]. Naturally, with the discovery of the Higgs boson [1,2], the NMSSM has drawn a lot attention, in general, to study the Higgs sector and the corresponding

[*]guchait@tifr.res.in
[†]jka@tifr.res.in

phenomenology in more detail at the LHC with great interest [12–14,17–20]. Previous studies showed that in the NMSSM framework, the scenario of very light Higgs bosons (< 125 GeV) exist, while one of the CP-even neutral Higgs bosons is SM-like [13,14,21–24]. Notably, these light Higgs bosons are non-SM-like and dominantly singlet in nature and, hence, not excluded by any past experiments due to the suppression of their production in colliders. Needless to say, in the present context of continuing Higgs studies in the LHC experiments, it is one of the priorities to search for these light non-SM-like Higgs bosons.

Already, in run 1 experiments at the LHC, extensive searches were carried out for the lightest CP-odd Higgs boson (A_1) either producing it directly or via the decay of the SM-like Higgs boson, $H_{\rm SM} \to A_1 A_1$. The CMS experiment performed searches through direct production of A_1 and decaying to a pair of muons [25] and taus [26] for the mass ranges 5.5–14 and 25–80 GeV respectively and, also looked for it in the SM Higgs decay in 4τ final states [26]. The ATLAS collaboration published results for A_1 searches, $H_{\rm SM} \to A_1 A_1 \to \mu\mu\tau\tau$ decays with a mass range 3.7–50 GeV [27] and also in four photon final states corresponding to the mass range 10–62 GeV [28]. From the nonobservation of any signal in all those searches, the exclusion of cross sections folded with branching ratios (BR) for a given channel are presented for the mass range ~5–60 of A_1.

On the phenomenological side, after the discovery of the Higgs boson at the LHC, detection prospects of all Higgs bosons in the NMSSM are revisited [29–31]. Nonetheless, it is more demanding to explore the detection possibility of the light non-SM-like Higgs bosons in various interesting decay channels to establish the NMSSM effects which are absent in the MSSM. In this context, searching for lighter Higgs bosons, in particular A_1 is very interesting and challenging [32,33]. There are many phenomenological analyses reported in the literature exploring the detection prospect of A_1 at the LHC [34–39]. In our study as reported in [21], the rates of production of non-SM-like Higgs bosons in various decay channels are estimated for the LHC run 2 experiment with the center of mass energy, $\sqrt{S} = 13$ TeV. Remarkably, it is observed that along with the dominant $b\bar{b}$ and $\tau\tau$ decay modes of non-SM-like Higgs bosons, the BR for two photon ($\gamma\gamma$) decay mode is also very large for a certain part of the parameter space. In particular, light A_1 decays to $\gamma\gamma$ mode with a BR ranging from a few percent to 80%–90% for a substantial region of the parameter space [19,21,39–43]. On the other side, as we know, experimentally photon is a very clean object and can be reconstructed with a very high precision, which motivates us to study the signal of non-SM-like Higgs boson in this $\gamma\gamma$ channel [33,39,44]. In this context, it is to be noted that neither the SM nor the MSSM predict this large rate of $\gamma\gamma$ decay mode of any of the Higgs bosons for any region of the parameter space. Hence, this distinct feature appears to be the robust signal of the NMSSM for a certain region of parameter space and can be exploited in distinguishing it from the other SUSY models. More precisely, in the presence of any SUSY signal, this diphoton decay mode of A_1 can be used as a powerful tool to establish the type of the SUSY model, provided parameter space is such that the BR$(A_1 \to \gamma\gamma)$ is large.

In this present study, mainly we focus on A_1 and explore its detection possibility in the $\gamma\gamma$ mode. In principle, A_1 can be produced directly via the standard SUSY Higgs production mechanisms, i.e. primarily via the gluon gluon fusion or through b and $\bar{b}$ annihilation. However, in both the cases, the production cross sections are suppressed due to its singlet nature. In our study, we employ the SUSY particle production, namely the associated chargino-neutralino and the subsequent decay of the heavier neutralino state produces A_1, followed by $A_1 \to \gamma\gamma$ decay. The combinations of lighter chargino ($\tilde{\chi}_1^\pm$) and either of the second ($\tilde{\chi}_2^0$) or the third ($\tilde{\chi}_3^0$) neutralino states are found to be produced dominantly at the LHC energy [45,46]. In the final state, in order to control the SM backgrounds, we require also one associated lepton arising from $\tilde{\chi}_1^\pm$ decay. The production and decay mechanism of the entire process is

$$\begin{array}{ccccc} pp \to & \tilde{\chi}_1^\pm & + & \tilde{\chi}_j^0 \ , \ (j=2,3) & \\ & \hookrightarrow \ \tilde{\chi}_1^0 \ell^\pm \nu & & \hookrightarrow \ \tilde{\chi}_1^0 \ A_1 & \\ & & & \hookrightarrow \ \gamma\gamma & \end{array} \tag{1.2}$$

schematically presented in Fig. 1. The final state contains hard missing energy due to the presence of neutrinos and neutralinos ($\tilde{\chi}_1^0$) which are assumed to be the lightest SUSY particle (LSP) and stable,[1] and escape the detector, since they are weakly interacting. Finally, the reaction, Eq. (1.2), leads to the signal,

$$\gamma\gamma + \ell^\pm + \not{E}_T. \tag{1.3}$$

Of course, in addition to the chargino-neutralino production cross section, the BR$(\tilde{\chi}_{2,3}^0 \to \tilde{\chi}_1^0 A_1)$ and BR$(A_1 \to \gamma\gamma)$, which are sensitive to the parameter space, are very crucial in determining the signal rate. In view of this, we investigate the sensitivity of this signal to the relevant parameters scanning those systematically for a wide range and identify the suitable region which provides the detectable rate of the signal for a given luminosity option. Finally, out of this parameter scan, we select a few benchmark parameter points for which results are presented. Performing a detailed simulation including detector effects for both

[1]We are considering the R-parity conserving model.

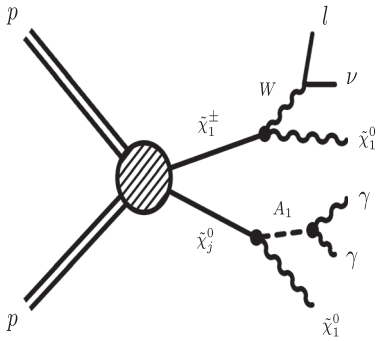

FIG. 1. Lighter chargino ($\tilde{\chi}_1^{\pm}$)-neutralino ($\tilde{\chi}_j^0$), ($j = 2, 3$) associated production in proton-proton collision followed by cascade decays to two photons and a lepton along with lightest neutralinos, as Eq. (1.2).

the signal and the SM backgrounds processes, we predict the signal significance corresponding to our choices of parameters for a few integrated luminosity options at the LHC with the center of mass energy, $\sqrt{S} = 13$ TeV.

This paper is organized as follows, In Sec. II, after briefly discussing the chargino and neutralino sector in the NMSSM, we study the parameter space sensitivity of chargino-neutralino associated production cross section. The parameter sensitivity of BRs of neutralinos and A_1 decays are discussed in Sec. III and then we propose a few benchmark points for which results are presented. The details of the simulation are presented in Sec. IV, while results are discussed in Sec. V. Finally, we summarize in Sec. VI.

II. CHARGINO-NEUTRALINO PRODUCTION

The chargino-neutralino associated production ($\tilde{\chi}_1^{\pm}\tilde{\chi}_{2,3}^0$) in proton-proton collision is mediated purely by electroweak (EW) interaction at the tree level and, hence, very sensitive to the parameters space owing to the dependence of couplings. Therefore, in order to understand the various features of this production process at the LHC, it is worth discussing the interplay between parameters and $\tilde{\chi}_1^{\pm}\tilde{\chi}_{2,3}^0$ production cross section.

A. Chargino and neutralino sector in NMSSM

In the SUSY model, there are spin half EW gauginos and Higgsinos which are the supersymmetric partners of the gauge bosons and Higgs bosons, respectively. The spontaneous breaking of EW symmetry lead a mixing between gaugino and Higgsino states making them weak eigenstates without physical mass terms. The charginos are the mass eigenstates corresponding to the mixed charged gaugino and Higgsino states. Similarly, the mixings of neutral EW gauginos and Higgsinos produce physical neutralinos. The masses and the corresponding physical states can be obtained by diagonalizing the respective mass matrices. For instance, the masses of the chargino states ($\tilde{\chi}_{1,2}^{\pm}$) are obtained diagonalizing the 2×2 chargino mass matrix by a biunitary transformation. In the MSSM, the masses and composition of these chargino states are determined by M_2—the SU(2) gaugino mass parameter, μ and $\tan\beta$—the ratio of two vacuum expectation values (v_u, v_d) of the neutral components of two Higgs doublets required to break EW symmetry spontaneously. In the NMSSM, the presence of an extra Higgs singlet field does not modify the chargino sector, hence it remains the same as in the MSSM, except the Higgsino mass parameter μ which is replaced by $\mu_{\rm eff}$.

On the contrary, in the NMSSM, the neutralino sector is extended due to the addition of an extra singlino state $\tilde{S}$—the fermionic superpartner of the singlet scalar field (S). Here $\tilde{S}$ mixes with the Higgsinos due to the presence of the $\lambda H_u H_d S$ term in the superpotential. Thus, the resulting $\mathbf{5} \times \mathbf{5}$ neutralino mass matrix is given by

$$M_N = \begin{pmatrix} M_1 & 0 & \frac{-g_1 v c_\beta}{\sqrt{2}} & \frac{g_1 v s_\beta}{\sqrt{2}} & 0 \\ 0 & M_2 & \frac{g_2 v c_\beta}{\sqrt{2}} & \frac{-g_2 v s_\beta}{\sqrt{2}} & 0 \\ \frac{-g_1 v c_\beta}{\sqrt{2}} & \frac{g_2 v c_\beta}{\sqrt{2}} & 0 & -\mu_{\rm eff} & -\lambda v s_\beta \\ \frac{g_1 v s_\beta}{\sqrt{2}} & \frac{-g_2 v s_\beta}{\sqrt{2}} & -\mu_{\rm eff} & 0 & -\lambda v c_\beta \\ 0 & 0 & -\lambda v s_\beta & -\lambda v c_\beta & 2\kappa v_s \end{pmatrix}. \quad (2.1)$$

Here M_1 is the mass of U(1) gaugino—the bino ($\tilde{B}$) and g_1, g_2 are the weak gauge couplings. In the MSSM limit, i.e. λ, $\kappa \to 0$, this 5×5 neutralino mass matrix reduces to a 4×4 mass matrix. The masses of neutralinos can be derived by diagonalizing symmetric matrix M_N via a unitary transformation as

$$M_{\tilde{\chi}^0}^D = N^* M_N N^\dagger, \quad (2.2)$$

with N as a unitary matrix. The analytical solution of the neutralino mass matrix presenting the spectrum of neutralino masses and mixings exist in the literature for the MSSM [47,48]. However for the NMSSM, the fifth order eigenvalue equation makes it more difficult to extract an exact analytical solution. Nevertheless, attempts are there to find the approximate analytical solution [49,50]. Consequently, the five physical neutralino states become the admixtures of weak states, such as gauginos, Higgsinos and singlino. Hence, in the basis $\tilde{\psi}^0 \equiv (-i\tilde{B}, -i\tilde{W}_3, \tilde{H}_d^0, \tilde{H}_u^0, \tilde{S})$, the physical neutralino states are composed of

$$\tilde{\chi}_i^0 = N_{ij}\tilde{\psi}_j^0, \quad (2.3)$$

where N_{ij} ($i, j = 1$–5) is defined by Eq. (2.2). In particular, N_{i5} presents the singlino component in the ith physical

neutralino state. To conclude, in the NMSSM, the masses and the mixings of the charginos and neutralinos at the tree level can be determined by six parameters, namely,

$$M_1, \qquad M_2, \qquad \tan\beta, \qquad \mu_{\rm eff}, \qquad \lambda, \qquad \kappa. \quad (2.4)$$

Here one can choose M_1 and M_2 to be real and positive by absorbing phases in $\tilde{B}^0$ and $\tilde{W}^0$ respectively, but in general $\mu_{\rm eff}$ can be complex. In this current study, we assume CP-conserving NMSSM setting all the input parameters real.

A careful examination of the neutralino mass matrix reveals a few characteristic features of this sector [49,50]. For instance, notice that the singlino field does not mix with the gaugino fields, and hence the singlino-like neutralino states do not interact with the gaugino-like states or gauge fields. Apparently, two out of the five neutralino states remain to be gaugino-like if $|M_{1,2} - \mu_{\rm eff}| > M_Z$. Note that the direct singlet-doublet mixing is determined by λ. The mass of the singlino-like neutralino is given by $|2\kappa v_s|$, and if $|2\kappa v_s| \ll M_{1,2}$, $\mu_{\rm eff}$, then the lighter neutralino state becomes dominantly a singlino-like. On the other hand, if $|2\kappa v_s| \gg M_{1,2}$, $\mu_{\rm eff}$, then the singlino state completely decouples from the other states resulting in all four neutralino states mixtures of gaugino-Higgsino, i.e. a MSSM-like scenario, whereas the remaining heavier neutralino state appears to be completely singlino-like. The coupling structures of neutralinos with gauge bosons and fermions remain the same as in the MSSM, since the singlet field does not interact with them directly. For the sake of discussion in the later section, we present the $\tilde{\chi}_1^\pm - \tilde{\chi}_j^0 - W^\mp$ interaction,

$$g^L_{\tilde{\chi}_1^\pm \tilde{\chi}_j^0 W^\mp} = \frac{e}{s_w}\left(N_{j2}V^*_{11} - \frac{1}{\sqrt{2}}N_{j4}V^*_{12}\right),$$
$$g^R_{\tilde{\chi}_1^\pm \tilde{\chi}_j^0 W^\mp} = \frac{e}{s_w}\left(N^*_{j2}U_{11} + \frac{1}{\sqrt{2}}N^*_{j3}U_{12}\right), \quad (2.5)$$

and $q - \tilde{q} - \tilde{\chi}_j^0$ couplings,

$$g^L_{d\tilde{d}\tilde{\chi}_j^0} \approx \frac{-e}{\sqrt{2}s_w c_w}\left(\frac{1}{3}N_{j1}s_w - N_{j2}c_w\right), \qquad g^R_{d\tilde{d}\tilde{\chi}_j^0} \approx 0, \quad (2.6)$$

$$g^L_{u\tilde{u}\tilde{\chi}_j^0} \approx \frac{-e}{\sqrt{2}s_w c_w}\left(\frac{1}{3}N_{j1}s_w + N_{j2}c_w\right), \quad g^R_{u\tilde{u}\tilde{\chi}_i^0} \approx 0, \quad (2.7)$$

with $s_w = \sin\theta_w$, $c_w = \cos\theta_w$ and $j = 2, 3$. Note that since we consider only the first two generations of squarks and assume that the chiral mixings are negligible, hence we omit the corresponding interaction terms and, for the same reasons, $g^R_{u\tilde{u}\tilde{\chi}_j^0}$ and $g^R_{d\tilde{d}\tilde{\chi}_j^0}$ are negligible. Apparently, the presence of the direct effect of NMSSM through the singlino component is absent in these interactions. However, because of the unitarity of the mixing matrix N, the singlino component N_{i5} indirectly affects these couplings. It will be discussed more in the next subsection in the context of the chargino-neutralino production.

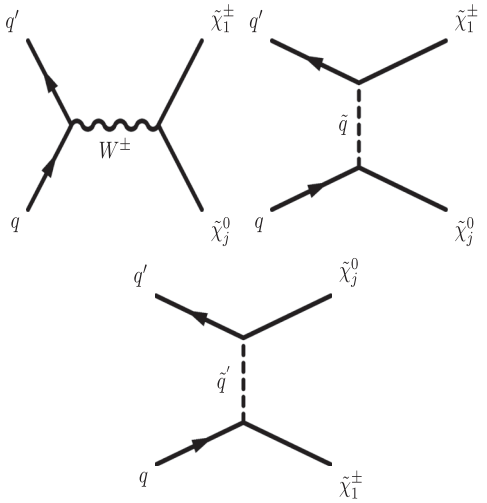

FIG. 2. Tree level Feynman diagrams for chargino-neutralino associated production via q and $\bar{q}'$ annihilation.

B. $\tilde{\chi}_1^\pm \tilde{\chi}_j^0$ cross section

In this section, in the framework of the NMSSM, we discuss various features of the chargino-neutralino ($\tilde{\chi}_1^\pm \tilde{\chi}_j^0$, $j = 1, 2, 3$) associated production at the LHC. For the sake of comparison and discussion, we also study $\tilde{\chi}_1^\pm \tilde{\chi}_1^0$ production cross section, although it has no relevance to our present context. As already mentioned, in hadron colliders, the chargino-neutralino pairs are produced purely via EW interaction initiated by quark and antiquark annihilation as

$$q\bar{q}' \to \tilde{\chi}_1^\pm \tilde{\chi}_j^0; \qquad j = 1, 2, 3, \quad (2.8)$$

the corresponding Feynman diagrams at the tree level are shown in Fig. 2. The s and t/u channels are mediated by the W boson and the first two generations of squarks respectively and are very sensitive to the couplings, see Eqs. (2.5)–(2.7), which are regulated by model parameters. In case, if both the chargino and the neutralino states be pure Higgsino-like, then the t and u channel diagrams decouple completely due to the suppressed quark-squark-neutralino couplings [Eqs. (2.6) and (2.7)], otherwise mixed or pure gaugino-like states are favored. The contribution of the t/u-channel diagrams are also suppressed for heavier masses of squarks. Moreover, negative interference of the s and t/u-channel diagrams yield an enhancement of the production cross section for heavier masses of squarks for a given set of other parameters.

The partonic level differential $\tilde{\chi}_1^\pm \tilde{\chi}_j^0$ cross section in NMSSM can be obtained following the form given in Ref. [51] for the MSSM,

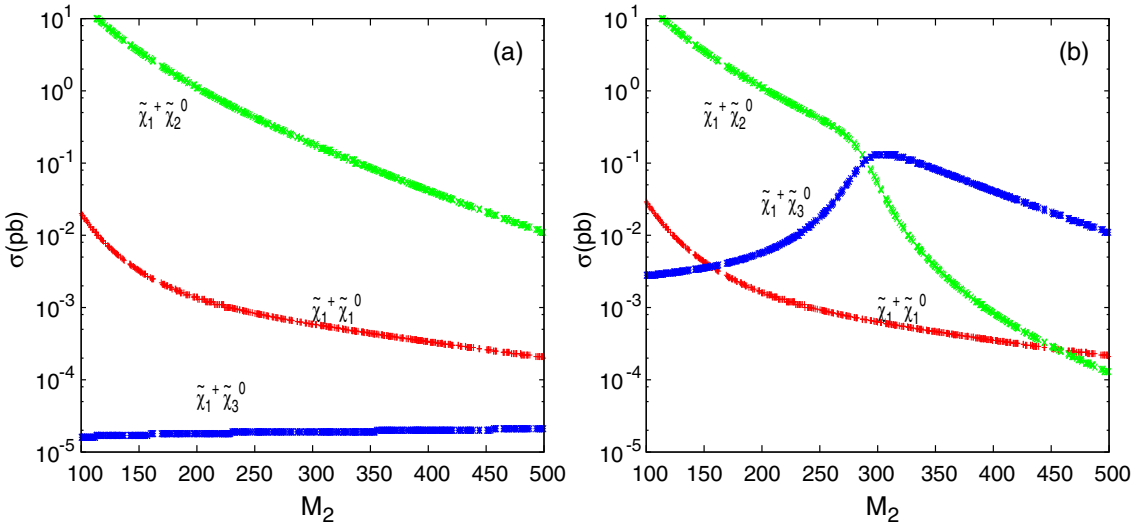

FIG. 3. Variation of leading order (LO) chargino-neutralino associated production cross section with M_2, at the LHC energy $\sqrt{S} =$ 13 TeV and for two choices of λ, $\kappa = (a)$ 0.1, 0.7, (b) 0.7, 0.1. The other parameters are set as, $\mu_{\rm eff} = 1000$ GeV, $M_1 = M_2/2$, $\tan\beta = 10$.

$$\frac{d\hat{\sigma}(q\bar{q} \to \tilde{\chi}_i^{\pm}\tilde{\chi}_j^0)}{d\hat{t}} = \frac{\pi\alpha^2}{3\hat{s}^2}\left[|Q_{\rm LL}|^2(\hat{u} - m^2_{\tilde{\chi}_j^0})(\hat{u} - m^2_{\tilde{\chi}_i^-}) + |Q_{\rm LR}|^2(\hat{t} - m^2_{\tilde{\chi}_j^0})(\hat{t} - m^2_{\tilde{\chi}_i^-}) + 2\hat{s}{\rm Re}(Q^*_{\rm LL}Q_{\rm LR})m_{\tilde{\chi}_j^0}m_{\tilde{\chi}_i^-}\right] \tag{2.9}$$

which is expressed in terms of four helicity charges $Q_{\rm LL}$, $Q_{\rm LR}$, $Q_{\rm RL}$, $Q_{\rm RR}$. For the sake of completeness, we also present the explicit form of these charges [51],

$$\begin{aligned}
Q_{\rm LL} &= \frac{1}{\sqrt{2}s_w^2}\left[\frac{N^*_{j2}V_{i1} - 1/\sqrt{2}N^*_{j4}V_{i2}}{\hat{s} - M_W^2} + V_{i1}\frac{I_{3\tilde{q}}N^*_{j2} + (e_{\tilde{q}} - I_{3\tilde{q}})N^*_{j1}\tan\theta_w}{\hat{u} - m^2_{\tilde{q}}}\right],\\
Q_{\rm LR} &= \frac{1}{\sqrt{2}s_w^2}\left[\frac{N_{j2}U^*_{i1} + 1/\sqrt{2}N_{j3}U^*_{i2}}{\hat{s} - M_W^2} - (U_{i1})^*\frac{I_{3\tilde{q}'}N_{j2} + (e_{\tilde{q}'} - I_{3\tilde{q}'})N_{j1}\tan\theta_w}{\hat{t} - m^2_{\tilde{q}'}}\right],\\
Q_{\rm RR} &= Q_{\rm RL} = 0,
\end{aligned} \tag{2.10}$$

where the Mandelstam variables are defined as $\hat{s} = (p_1 + p_2)^2$; $\hat{t} = (p_1 - p_3)^2$; $\hat{u} = (p_2 - p_4)^2$ in the partonic frame, p_1, p_2 are the momenta of initial quarks, p_3, p_4 represent the same for $\tilde{\chi}_i^{\pm}$ and $\tilde{\chi}_j^0$ respectively. Notice that, as pointed out earlier, even without any explicit dependence of couplings, Eqs. (2.5)–(2.7), on the singlino composition, N_{j5} in the neutralino state, nonetheless, it affects the $\tilde{\chi}_1^{\pm}\tilde{\chi}_j^0$ production cross section due to the dilution of gaugino and Higgsino components.

We compute this leading order (LO) cross section setting QCD scales, $Q^2 = \hat{s}$ the partonic center of mass energy and for the choice of CT10 [52] parton distribution function. The corresponding next to leading order (NLO) predictions for the $\tilde{\chi}_1^{\pm}\tilde{\chi}_j^0$ cross sections are obtained from Prospino [53] and the k-factor ($= \sigma_{\rm NLO/\sigma_{LO}}$) is found to be $\sim$1.3 [51]. In the present NMSSM case, to take care NLO effects in cross section, we use the same k-factor, which is not expected to be significantly different with respect to the MSSM case. We observe that LO chargino-neutralino associated production cross section varies from subfemtobarn (fb) level to few picobarn (pb) for the mass range of 100–500 GeV of charginos and neutralinos.

To understand the dependence of $\tilde{\chi}_1^{\pm}\tilde{\chi}_j^0$ cross sections on the parameters, we demonstrate its variation in Figs. 3 and 4, primarily for gaugino- and Higgsino-like scenarios varying M_2 and $\mu_{\rm eff}$ respectively. The variation of singlino composition is controlled by a set of a few choices of λ, $\kappa = (a)0.1, 0.7$, (b) 0.2,0.1 for Fig. 3 and $\lambda, \kappa =$ (a) 0.7, 0.1, (b) 0.2, 0.1 and (c) 0.4, 0.1 for Fig. 4. The other parameters are set as $\tan\beta = 10$, $\mu_{\rm eff} = 1000$ GeV (for Fig. 3), $M_2 = 600$ GeV (for Fig. 4), squark masses $m_{Q_{\rm L}}$, $m_{D_{\rm L,R}} =$ 1000 GeV and assuming the relation $M_1 = M_2/2$. In the following, we discuss the variation of cross sections with the sensitive parameters which has some impact on the signal sensitivity, as will be discussed in the later sections.

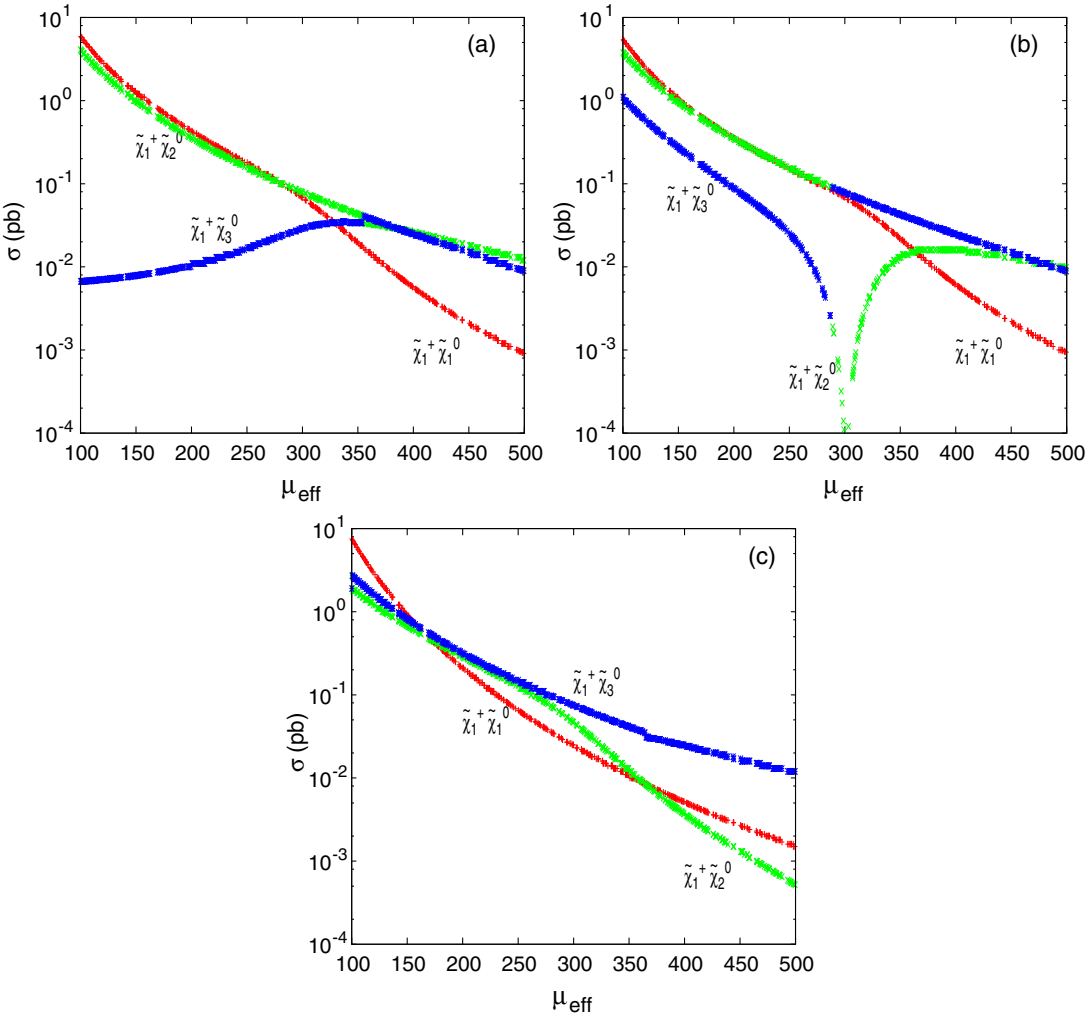

FIG. 4. Variation of LO chargino-neutralino associated production cross section with $\mu_{\rm eff}$, at the LHC energy $\sqrt{S} = 13$ TeV and for the choices of λ, κ = (a) 0.1, 0.7, (b) 0.2, 0.1, (c) 0.4, 0.1. The other parameters are set as $M_2 = 600$ GeV, $M_1 = M_2/2$, $\tan\beta = 10$.

(i) The dependence of $\tilde{\chi}_1^\pm\tilde{\chi}_j^0$ cross section on M_2, in the gaugino-like scenario ($M_2 < \mu_{\rm eff} = 1000$ GeV) is presented in Fig. 3. In this scenario, in the case of $\lambda, \kappa = (a)\ 0.1, 0.7$, the mass of singlino is very heavy ($\sim|2\kappa v_s| = 2\mu_{\rm eff}\kappa/\lambda = 14$ TeV) and the $\tilde{\chi}_1^\pm$ state is wino-like of mass around M_2, while the $\tilde{\chi}_1^0$ is bino dominated with its mass about $m_{\tilde{\chi}_1^0} \sim M_1$. On the other hand, because of the large mass of the singlino state and lower value of λ, i.e. small singlet-doublet mixing, the $\tilde{\chi}_2^0$ and $\tilde{\chi}_3^0$ states turn out to be dominantly wino- and Higgsino-like respectively, with masses $m_{\tilde{\chi}_2^0} \sim M_2$ and $m_{\tilde{\chi}_3^0} \sim \mu_{\rm eff}$. It explains the larger cross section for $\tilde{\chi}_1^\pm\tilde{\chi}_2^0$ in comparison to the combination $\tilde{\chi}_1^\pm\tilde{\chi}_1^0$, as seen in Fig. 3(a). Note that the subsequent fall of both cross sections with the increase of M_2 is purely a mass effect. Obviously, the $\tilde{\chi}_1^\pm\tilde{\chi}_3^0$ cross section is expected to be suppressed and almost negligible dependence on M_2. However, in the case of λ, $\kappa = (b)\ 0.7, 0.1$, the singlino state becomes comparatively light with mass about ~300 GeV. In this scenario, due to the large singlet-doublet mixing ($\lambda = 0.7$), at the lower values of M_2, the $\tilde{\chi}_3^0$ state is found to be singlino-like with very less wino and Higgsino components, whereas $\tilde{\chi}_2^0, \tilde{\chi}_1^0$ states appear to be more or less wino- and bino-like respectively. Consequently, in this lower region of M_2, the $\tilde{\chi}_1^\pm\tilde{\chi}_{1,2}^0$ cross sections are higher than the $\tilde{\chi}_1^\pm\tilde{\chi}_3^0$, mainly due to the suppressed couplings of $\tilde{\chi}_3^0$ with gauge boson and fermions being a dominantly singlino state. However, with the increase of M_2, the wino (singlino) component in $\tilde{\chi}_2^0$ ($\tilde{\chi}_3^0$) decreases, resulting a gradual fall (enhancement) of $\tilde{\chi}_1^\pm\tilde{\chi}_2^0$ ($\tilde{\chi}_1^\pm\tilde{\chi}_3^0$) cross sections. Eventually, as M_2 reaches closer to $|2\kappa v_s| \sim 300$ GeV, the $\tilde{\chi}_2^0$ and $\tilde{\chi}_3^0$ states tend to be singlino-like and wino-like respectively and, hence, due to the depletion of $\tilde{\chi}_1^\pm\tilde{\chi}_2^0$ cross section very sharply, $\tilde{\chi}_1^\pm\tilde{\chi}_3^0$ cross section takes

over it and then falls slowly mainly due to the phase space suppression, see Fig. 3(b). However, in contrast, due to the larger mass of singlino (∼14 TeV) the similar type of crossing between $\tilde{\chi}_1^{\pm}\tilde{\chi}_2^0$ and $\tilde{\chi}_1^{\pm}\tilde{\chi}_3^0$ cross sections is not observed in Fig. 3(a).

(ii) The variation of cross sections with $\mu_{\rm eff}$, for the Higgsino-like scenario is presented in Fig. 4, keeping $M_2 = 600$ GeV and for three combinations of λ, $\kappa = (a)$ 0.1, 0.7, (b) 0.2, 0.1, (c) 0.4, 0.1. In this scenario, the $\tilde{\chi}_1^{\pm}$ state is mostly Higgsino-like for the lower range of $\mu_{\rm eff}$, and later becomes a gaugino-Higgsino mixed state when $\mu_{\rm eff} \sim M_2$. For scenario (a), at the lower range of $\mu_{\rm eff}$ ($\lesssim M_1 = 300$ GeV), the Higgsino composition in the $\tilde{\chi}_1^0$ state is the dominant one, but it becomes bino-like once $\mu_{\rm eff} \gtrsim M_1$ and a drop of $\tilde{\chi}_1^{\pm}\tilde{\chi}_1^0$ cross section occurs beyond $\mu_{\rm eff} \sim 300$ GeV, as seen in Fig. 4(a). However, for scenarios (b) and (c), at the lower side of $\mu_{\rm eff}$, the $\tilde{\chi}_1^0$ state, along with some Higgsino component, contains a finite fraction of singlino (recall the singlino mass $\sim 2\mu_{\rm eff}\kappa/\lambda$), and in particular, for the scenario (c), $\tilde{\chi}_1^0$ becomes dominantly singlino-like. Nevertheless, the $\tilde{\chi}_1^{\pm}\tilde{\chi}_1^0$ cross sections are not heavily suppressed due to the presence of the mild Higgsino component in the $\tilde{\chi}_1^0$ state. The Higgsino- and bino-like nature of $\tilde{\chi}_2^0$ yields a steady variation of $\tilde{\chi}_1^{\pm}\tilde{\chi}_2^0$ cross section with $\mu_{\rm eff}$, except for case (b) where a sudden drop and then further an enhancement is observed at $\mu_{\rm eff} \sim 300$ GeV. Here both the singlino and the bino masses are around ∼300 GeV, implying an increase of singlino and bino components in the $\tilde{\chi}_2^0$ state causing a drop of $\tilde{\chi}_1^{\pm}\tilde{\chi}_2^0$ cross section and beyond this region, again it goes up with the increase of $\mu_{\rm eff}$ due to further increase of its Higgsino component. In the presence of small singlet-doublet mixings, in the scenario λ, $\kappa = (a)$ 0.1, 0.7, the $\tilde{\chi}_3^0$ state is bino dominated at the lower range of $\mu_{\rm eff} < M_1$, resulting in a comparatively lower $\tilde{\chi}_1^{\pm}\tilde{\chi}_3^0$ cross section, which slowly increases with $\mu_{\rm eff}$ due to the enhancement of Higgsino composition in it, as observed in Fig. 4(a). In Fig. 4(b), it is found that the singlino composition in the $\tilde{\chi}_3^0$ state goes up with the increase of $\mu_{\rm eff}$, while it is below $|2\kappa v_s|$ and becomes completely singlino-like at $\mu_{\rm eff} \sim |2\kappa v_s|$ (∼300 GeV) hence the rapid fall of the $\tilde{\chi}_1^{\pm}\tilde{\chi}_3^0$ cross section. Beyond $\mu_{\rm eff} > 2|\kappa v_s|$ region, Higgsino composition in the $\tilde{\chi}_3^0$ state increases yielding more higher $\tilde{\chi}_1^{\pm}\tilde{\chi}_3^0$ cross section and then due to mass effect, it falls slowly.

III. DECAYS: $\tilde{\chi}_{2,3}^0 \to \tilde{\chi}_1^0 A_1$; $A_1 \to \gamma\gamma$

As stated earlier, the sensitivity of the signal $\ell + \gamma\gamma + \not{E}_T$ crucially depends on the combined effects of the $\tilde{\chi}_1^{\pm}\tilde{\chi}_{2,3}^0$ production cross section and subsequent BRs involved in the cascade decays, such as $\tilde{\chi}_{2,3}^0 \to \tilde{\chi}_1^0 A_1$ and $A_1 \to \gamma\gamma$, $\tilde{\chi}_1^{\pm} \to \tilde{\chi}_1^0 \ell\nu$. Note that the BR($\tilde{\chi}_1^{\pm} 1 \to \tilde{\chi}_1^0 \ell^{\pm}\nu$) is almost the same as the leptonic BR of W-boson for our considered parameter space.

In this section, the sensitivity of signal, Eq. (1.3) cross sections with the parameters are studied systematically using NMSSMTools4.9.0 [54] taking into account various constraints such as dark matter, flavor physics and direct searches at LEP and LHC experiments. In this numerical scan we use the following range of parameters:

$$\begin{aligned} &0.1 < \lambda < 0.7; \quad 0.1 < \kappa < 0.7; \\ &0 < A_\lambda < 2\ \text{TeV}, \quad -9 < A_\kappa < -4\ \text{GeV}; \\ &2 < \tan\beta < 50; \quad 140\ \text{GeV} < \mu_{\rm eff} < 600\ \text{GeV} \\ &M_{Q_3} = M_{U_3} = 1\text{–}3\ \text{TeV}, \quad A_t = -3 - (+3)\ \text{TeV}. \end{aligned} \tag{3.1}$$

The other soft masses are set as

$$\begin{aligned} &M_{Q_{1/2}} = M_{U_{1/2}} = M_{D_{1/2}} = M_{D_3} = M_{L_3} = M_{E_3} = A_{E_3} = 1\ \text{TeV}, \\ &A_b = 2\ \text{TeV}, \quad M_{L_{1,2}} = M_{E_{1,2}} = 200\ \text{GeV}, \quad A_{E_{1,2}} = 0. \end{aligned}$$

The important factors in this discussion are the mass and the composition of A_1 which is dominantly singlet-like. In order to understand the variation of composition of A_1, here we briefly revisit the Higgs mass matrix corresponding to CP-odd states. The initial 3×3 CP-odd Higgs mass matrix reduces to a 2×2 matrix after rotating away the Goldstone mode. Hence, the CP-odd mass matrix, M_P^2, in the basis of doublet (A) and singlet (S), is given by [9,10]

$$M_P^2 = \begin{pmatrix} M_A^2 & \lambda(A_\lambda - 2\kappa v_s)v \\ \lambda(A_\lambda - 2\kappa v_s)v & M_S^2 \end{pmatrix}, \tag{3.2}$$

where

$$\begin{aligned} M_A^2 &= \frac{2\mu_{\rm eff}(A_\lambda + \kappa v_s)}{\sin 2\beta}, \\ M_S^2 &= \lambda(A_\lambda + 4\kappa v_s)\frac{v_u v_d}{v_s} - 3\kappa A_k v_s. \end{aligned} \tag{3.3}$$

This 2×2 mass matrix can be diagonalized by an orthogonal rotation with an angle α_A, as given by

$$\tan 2\alpha_A = \frac{2M_{12}^2}{(M_A^2 - M_S^2)}, \tag{3.4}$$

where $M_{12}^2 = \lambda(A_\lambda - 2\kappa v_s)v$ and $v = \sqrt{v_u^2 + v_d^2}$. Obviously, two mass eigenstates (A_1, A_2) are the mixtures of the doublet (A) and the singlet (S) weak eigenstates.

(i) $\tilde{\chi}_j^0 \to \tilde{\chi}_1^0 A_1$, $j = 2, 3$.—The relevant part of the coupling (Higgsino-Higgsino-Singlet) for this decay channel is given by

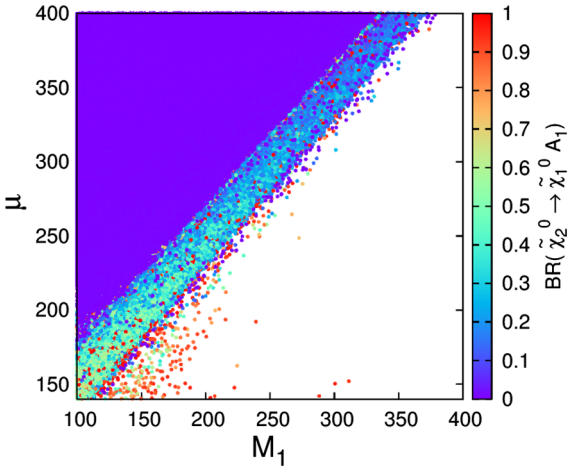

FIG. 5. $\mathrm{BR}(\tilde{\chi}_2^0 \to \tilde{\chi}_1^0 A_1)$ in the $M_1 - \mu_{\rm eff}$ plane. All energy units are in GeV.

$$g_{\tilde{\chi}_j^0 \tilde{\chi}_1^0 A_1} \approx \frac{i}{\sqrt{2}} \lambda P_{13}(N_{j4}N_{13} + N_{j3}N_{14}). \tag{3.5}$$

Here $P_{13} \sim \cos\alpha_A$ presents the singlino composition in A_1. Hence, for very small values of $\sin\alpha_A$ this coupling favors only the Higgsino-like $\tilde{\chi}_j^0$ and $\tilde{\chi}_1^0$ states. Note that, in the context of our signal, the gaugino-like $\tilde{\chi}_j^0$ and $\tilde{\chi}_1^0$ states are not favored in order to suppress the decay modes such as, $\tilde{\chi}_j^0 \to \tilde{\chi}_1^0 Z, \ell\bar{\ell}$. This type of Higgsino-like scenario can be achieved by setting $\mu_{\rm eff} \sim M_1 < M_2$, which also makes $\tilde{\chi}_{2,3}^0$ and $\tilde{\chi}_1^0$ states almost degenerate, i.e. $m_{\tilde{\chi}_2^0} \sim m_{\tilde{\chi}_1^0}$, resulting in a compressed-like scenario. However, in order to have a reasonable sensitivity of this signal, the visible decay spectrum is expected to be a little bit harder to pass kinematic thresholds, which can be ensured by setting the mass splitting, $\Delta m = m_{\tilde{\chi}_{2,3}^0} - m_{\tilde{\chi}_1^0} \sim 50$ GeV. This requirement leads us to choose M_1 less than $\mu_{\rm eff}$, but of course not by a huge gap to retain the sufficient Higgsino component, making $\tilde{\chi}_1^0$ a bino-Higgsino mixed state. In Fig. 5, we show the correlation of $\mathrm{BR}(\tilde{\chi}_2^0 \to \tilde{\chi}_1^0 A_1)$ in the $M_1 - \mu_{\rm eff}$ plane, setting slepton masses to 1 TeV. Notice that the 10% or more $\mathrm{BR}(\tilde{\chi}_2^0 \to \tilde{\chi}_1^0 A_1)$ corresponds to the region $M_1 \sim \mu_{\rm eff}$ and we found that it remains to be valid for a wide range of λ and κ. This figure clearly reflects the preferred choices of M_1 and $\mu_{\rm eff}$ for our considered signal channel.

(ii) $A_1 \to \gamma\gamma$.—The earlier studies [19,21,40,41] showed that the variation of BR of non-SM-like NMSSM Higgs bosons in various decay channels is very dramatic depending on the region of parameters. For instance, the singlet-like A_1 state decouples from the fermions leading a suppression of the tree level decay modes $b\bar{b}$ and $\tau\tau$ and an enhancement of $\mathrm{BR}(A_1 \to \gamma\gamma)$ channel [19,40,41]. The cause of having a finite partial $A_1 \to \gamma\gamma$ decay width can be understood by examining the respective coupling structures of A_1 with two photons [55]. The A_1 state decays to two photons via loops comprising heavy fermions and charginos [56,57], see Fig. 6. The partial decay width of $A_1 \to \gamma\gamma$ can be obtained simply using the MSSM expression, but replacing the respective couplings to the NMSSM values. Thus, it is given as [56,57]

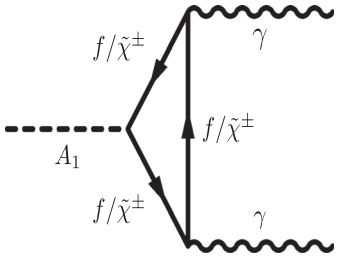

FIG. 6. Loop diagrams for the decay of A_1 to two photons, mediated by fermion (f) and chargino ($\tilde{\chi}^{\pm}$).

$$\Gamma(A_1 \to \gamma\gamma) = \frac{G_F \alpha_{em}^2 M_{A_1}^3}{32\sqrt{2}\pi^3} \left| \sum\nolimits_f N_c e_f^2 g_f^{A_1} A_f(\tau_f) + \sum\nolimits_{\tilde{\chi}_i^{\pm}} g_{\tilde{\chi}_i^{\pm}}^{A_1} A_{\tilde{\chi}_i^{\pm}}(\tau_{\tilde{\chi}_i^{\pm}}) \right|^2. \tag{3.6}$$

Here N_c is the QCD color factor, e_f is the electric charge of the fermions (f), $A_x(\tau_x)$ are the loop functions given by

$$A_x(\tau_x) = \tau_x \left(\sin^{-1} \frac{1}{\sqrt{\tau_x}} \right)^2, \qquad \tau_x = \frac{4M_x^2}{M_{A_1}^2}; \qquad x = f, \quad \tilde{\chi}_i^{\pm}. \tag{3.7}$$

Here $g_f^{A_1}$ are the couplings of A_1 with the heavier fermions (f = top and bottom quarks), where as $g_{\tilde{\chi}^{\pm}}^{A_1}$ are the same with charginos, and all those are given by [9]

$$g_u^{A_1} = -i \frac{m_u}{\sqrt{2} v \sin\beta} P_{12}, \qquad g_d^{A_1} = i \frac{m_d}{\sqrt{2} v \cos\beta} P_{11}, \tag{3.8}$$

$$g_{\tilde{\chi}_i^{\pm} \tilde{\chi}_j^{\mp} A_1} = \frac{i}{\sqrt{2}} [\lambda P_{13} U_{i2} V_{j2} - g_2 (P_{12} U_{i1} V_{j2} + P_{11} U_{i2} V_{j1})]. \tag{3.9}$$

Here P and (U, V) are the mixing matrices for pseudoscalar Higgs bosons and chargino sector

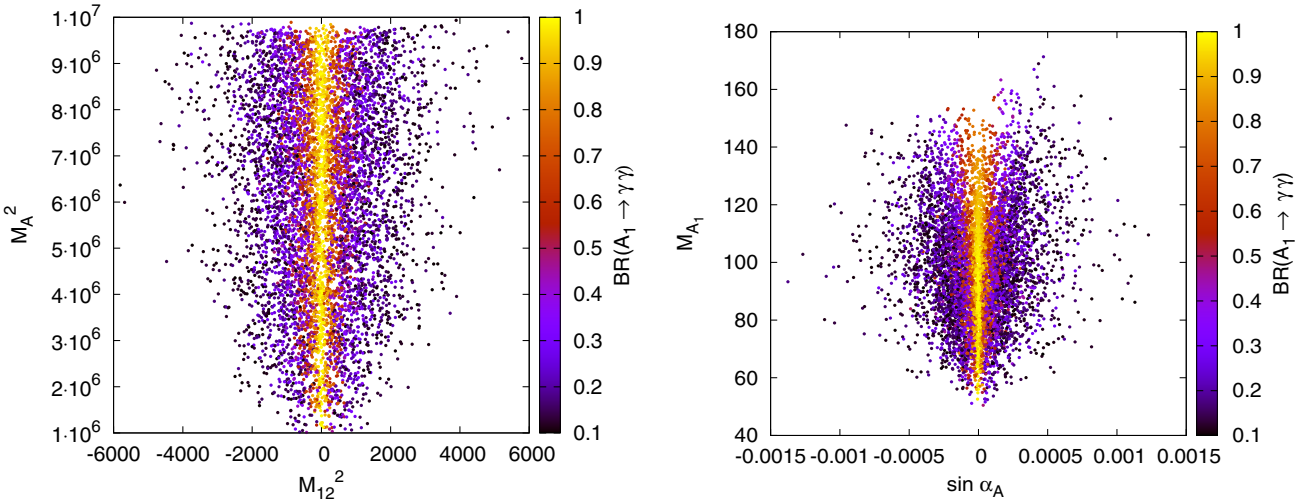

FIG. 7. $\mathrm{BR}(A_1 \to \gamma\gamma)$ in the $M_A^2 - M_{12}^2$ (left) and $\sin\alpha_A - M_{A_1}$ plane (right). The other parameters are varied for the range, as given in Eq. (3.1). All energy units are in GeV.

respectively and, in particular $P_{11} = \sin\alpha_A \sin\beta$ and $P_{12} = \sin\alpha_A \cos\beta$. In the pure singlet limit of $A_1(P_{11}, P_{12} \sim 0)$, see Eq. (2.6), and the fermion couplings ($g_u^{A_1}$, $g_d^{A_1}$) approach to almost negligible value ($\sim 10^{-5}$) and, hence, the corresponding fermionic loop contribution in Eq. (3.6) are extremely suppressed. On the other hand, the presence of Higgsino composition (U_{i2}, V_{j2}) in the chargino state yields an enhanced coupling with A_1 via the singlet-Higgsino-Higgsino interaction [see the term proportional to λ in Eq. (3.9)]. Needless to say that it is an effect beyond MSSM. Naturally, it is interesting to identify the region of the parameter space which offers a finite partial width of the $A_1 \to \gamma\gamma$ mode. We try to study it by examining the mixing of CP-odd Higgs boson states via the mass matrix, Eqs. (3.2) and (3.3). Recall that a very small value of $\sin\alpha_A$ leads a singlet dominated A_1 state resulting in a suppression of its couplings with the fermions. Following the mass matrix, it can be realized very easily that the lighter CP-odd state A_1 can be singlet-like in the presence of negligible mixing between A and S states. Essentially, it occurs due to the following two conditions:

1. $M_A^2 \gg M_S^2, M_{12}^2$ i.e. the heavier state is too heavy and purely doublet-like whereas the lighter state is singlet, a decoupled type of scenario.
2. $M_{12}^2 = (A_\lambda - 2\kappa v_s) \sim 0$, i.e., a cancellation between the two terms in the off-diagonal element.

These two scenarios are illustrated in Fig. 7, presenting the range of M_A^2 and M_{12}^2 [Eqs. (3.2) and (3.3)], corresponding to $\mathrm{BR}(A_1 \to \gamma\gamma) \gtrsim 10\%$. In the left panel, we present the range of the diagonal term M_A^2 and the off-diagonal element M_{12}^2 of the mass matrix M_P^2, Eq. (3.2). As expected, for very low values of $M_{12}^2(\sim 0)$ and corresponding to larger values of $M_A^2 \sim 10^6$, $\mathrm{BR}(A_1 \to \gamma\gamma)$ appears to be ($\gtrsim 80\%$), and even for the case $0 < |M_{12}^2| \ll M_A^2$, it can be about 10%–20%. It also indicates that the $\mathrm{BR}(A_1 \to \gamma\gamma)$ becomes almost 100% for the scenario $M_{12}^2 \sim 0$, i.e. $A_\lambda \sim 2\kappa v_s$. Moreover, we show the range of mixing angle in terms of $\sin\alpha_A$ and the mass of A_1 in Fig. 7 (right), corresponding to the range of M_{12}^2 and M_A^2, providing $\mathrm{BR}(A_1 \to \gamma\gamma) > 10\%$ as shown in the left panel of the same figure. It clearly confirms the smallness of the mixing angle responsible to yield a large $\mathrm{BR}(A_1 \to \gamma\gamma)$ and interestingly it occurs for a wide range of M_{A_1}. Similarly, corresponding to the range of parameters as shown in Fig. 7, for which $\mathrm{BR}(A_1 \to \gamma\gamma) \gtrsim 10\%$, the relevant range of A_λ and μ_{eff} is shown in the $\lambda - \kappa$ plane in the left and the right panel of Fig. 8 respectively. It is observed that reasonably wide ranges of $\lambda(0.1\text{–}0.4)$ and $\kappa(0.1\text{–}0.65)$ can provide a large $\mathrm{BR}(A_1 \to \gamma\gamma)$ for a larger range of A_λ and for a moderately large values of μ_{eff}. It is to be noted also that a preferably Higgsino-like lighter chargino, i.e. a smaller μ_{eff} as compared to M_2, is required in order to enhance the partial width of this channel.

Finally, based on the above observations about the parameter dependence of the production cross sections, $\mathrm{BR}(\tilde{\chi}_2^0 \to \tilde{\chi}_1^0 A_1)$ and $\mathrm{BR}(A_1 \to \gamma\gamma)$, we set up a few benchmark points (BPs) in order to present results. In summary, the preferred choices are, $\tilde{\chi}_1^0$ as a bino-Higgsino mixed state, $\tilde{\chi}_{2,3}^0$ and $\tilde{\chi}_1^\pm$ primarily Higgsino-like, i.e. $M_1 < \mu_{\mathrm{eff}}$, but not with a large gap between M_1 and μ_{eff}, and M_2 set to a larger value satisfying $M_2 > \mu_{\mathrm{eff}}$. In Table I, we show six BPs and present the corresponding parameters, masses of relevant particles and BRs. In order to make $\mathrm{BR}(\tilde{\chi}_2^0 \to \tilde{\chi}_1^0 A_1)$ dominant the decay mode $\tilde{\chi}_2^0 \to \tilde{l}l$ is suppressed by fixing slepton masses to higher values

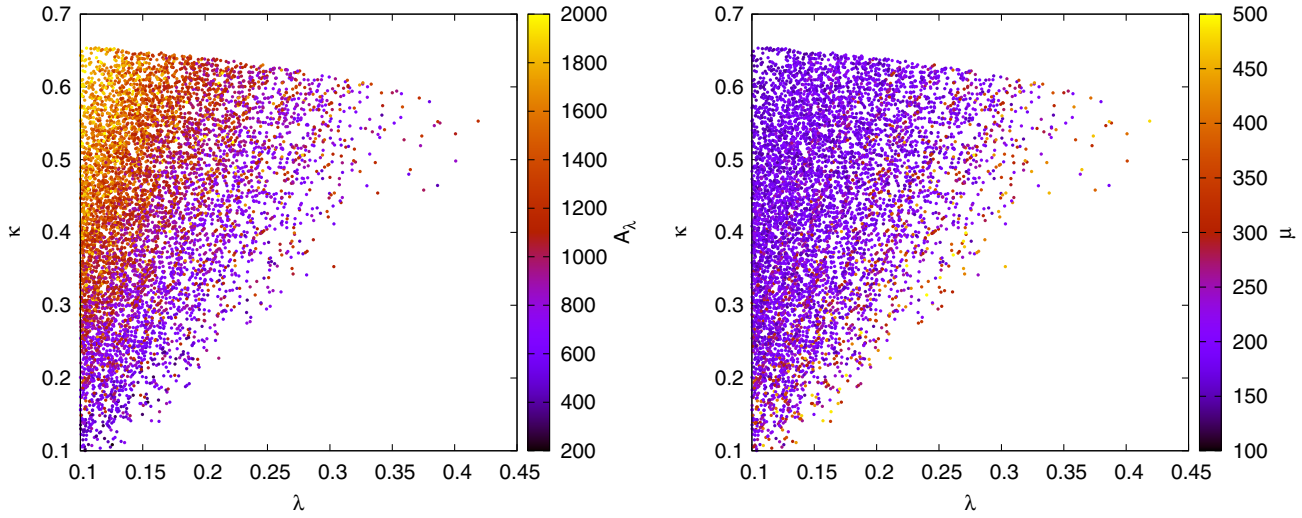

FIG. 8. BR($A_1 \to \gamma\gamma$) ($\geq 10\%$) in the $\lambda - \kappa$ plane for the range of A_λ (left) and $\mu_{\rm eff}$ (right). The other parameters are varied for the range, as given in Eq. (3.1).

which are not shown in this Table. Notice that BP1–BP4 present comparatively lighter masses of chargino and neutralino states, whereas these are massive for BP5 and BP6. The values of M_{A_1} are chosen in such a way that the decay of the SM Higgs to a pair of A_1 is forbidden in order to make it compatible with the recent SM Higgs boson results [58]. For all BPs the lightest CP-even Higgs boson H_1 is SM-like. Although, both the $\tilde{\chi}_2^0$ and $\tilde{\chi}_3^0$ neutralino states are Higgsino-like, more precisely the coupling strength depends on the kind of Higgsino composition, either it is $\tilde{H}_u$ or $\tilde{H}_d$ [see Eq. (3.5)] like.

TABLE I. Parameters, masses, and BRs for six benchmark points.

	BP1	BP2	BP3	BP4	BP5	BP6
λ	0.29	0.40	0.10	0.53	0.64	0.50
κ	0.37	0.45	0.20	0.39	0.36	0.48
$\tan\beta$	6.46	6.46	11.0	4.0	2.5	2.84
M_A	1722	340.7	1311.5	1262.4	1436.9	1655.8
A_κ	−4.97	−4.97	−3.9	−5.8	−6.5	−9.37
$\mu_{\rm eff}$	342.4	200.0	158.5	365.4	636.8	540.7
M_1	300	150.0	135.4	275.9	605.8	514.0
M_2	606.6	606.6	1000.0	9000	1857.4	1597.1
$M_{\tilde{\chi}_1^0}$	280.6	131.4	113.4	261.8	578.3	488.5
$M_{\tilde{\chi}_2^0}$	356.4	210.0	169.0	379.1	657.5	559.8
$M_{\tilde{\chi}_3^0}$	356.7	215.6	182.3	385.5	661.0	572.7
$M_{\tilde{\chi}_1^+}$	340.0	199.3	161.7	377.5	648.6	550.6
M_{A_1}	62	76	63.1	105.2	62.8	66.8
M_{H_1}	124	124	124	124	125	123
BR($\chi_2^0 \to \tilde{\chi}_1^0 A_1$)	0.92	0.83	0.0	0.44	0.98	0.05
BR($\chi_3^0 \to \tilde{\chi}_1^0 A_1$)	0.27	0.31	0.52	0.002	0.11	0.97
BR($A_1 \to \gamma\gamma$)	0.79	0.91	0.98	0.87	0.97	0.97

Notice that, for BP4, because of the higher mass of A_1, the $A_1 \to Z\gamma$ also opens up and BR is found to be around $\sim 2\%$. This decay channel of A_1, produced through the process Eq. (1.2), can give rise to a spectacular signal with the final state $Z\gamma$ along with a lepton and $\not{E}_T$.

IV. SIGNAL AND BACKGROUND

In this section we present the detection prospect of finding the signal $\gamma\gamma + \ell^\pm + \not{E}_T$ at the LHC with the center of mass energy, $\sqrt{S} = 13$ TeV, corresponding to a few integrated luminosity options. As mentioned in the previous section, the signal events appear from both the $\tilde{\chi}_1^\pm \tilde{\chi}_2^0$ and $\tilde{\chi}_1^\pm \tilde{\chi}_3^0$ production following the cascade decays, $\tilde{\chi}_{2,3}^0 \to \tilde{\chi}_1^0 A_1$, and $A_1 \to \gamma\gamma$ [Eq. (1.2)]. The lepton originates mainly from $\tilde{\chi}_1^\pm \to \ell^\pm \nu \tilde{\chi}_1^0$ decay and the missing transverse energy ($\not{E}_T$) arises due to the presence of massive LSPs, in addition to almost massless neutrinos. The dominant SM background contributions come from the following processes"

$$\text{pp} \to W\gamma, \qquad Z\gamma, \qquad W\gamma\gamma, \qquad Z\gamma\gamma, \tag{4.1}$$

with the leptonic decays of W/Z. Note that in the first two cases, the second photon originates primarily from the initial state, radiated by incoming quarks. In addition, the other potential sources of background are the processes,

$$\text{pp} \to W\gamma j, \qquad Z\gamma j, \tag{4.2}$$

where the second hard photon is arising from radiation, and interestingly, it is found to be the dominant ones.

In our simulation we generate signal events using PYTHIA6 [59] providing spectrum of SUSY particles

and BR of various decay channels through the SLHA file [60], obtained from NMSSMTools [54], corresponding to our chosen parameter space, as shown in Table I. The background events with two-body at the final state ($W\gamma$, $Z\gamma$) are generated directly using PYTHIA6, while processes consisting of three-body are simulated using the MadGraph [61] and then PYTHIA6 is used for showering. The generated events are stored in the standard HEP format (STDHEP) [62] to pass them through Delphes3.2.0 [63] to take into account the detector effects. In our analysis we have used the default CMS card in Delphes, but results are also checked with ATLAS default card and not many differences are observed.

The objects in the final state such as electron, photon and missing transverse energy are identified and reconstructed using Delphes based algorithms [63]. However, for the sake of completeness, we describe very briefly the object reconstruction techniques followed in the Delphes.

(i) *Lepton selection*.—The electrons are reconstructed using the information from the tracker and electromagnetic calorimeter(ECAL) parametrizing the combined reconstruction efficiency as a function of the energy and pseudorapidity. The muons are reconstructed using the predefined reconstruction efficiency and the final momentum is obtained by a Gaussian smearing of the initial 4-momentum vector. In our simulation, both the electrons and the muons are selected, imposing cuts on the transverse momenta (p_T^{ℓ}) and pseudorapidity (η^l) of the lepton as

$$p_T^{\ell} \geq 20\,\text{GeV}; \quad |\eta^l| \leq 2.5; \quad (l = e, \mu), \tag{4.3}$$

where η^{ℓ} restriction is due to the limited tracker coverage. The leptons are required to be isolated by demanding the total transverse energy $E_T^{ac}(\ell) \leq 20\%$ of the p_T^{ℓ}, where $E_T^{ac}(\ell)$ is the scalar sum of transverse energies of particles with minimum transverse momentum 0.5 GeV around the lepton direction within a cone size of $\Delta R = 0.5$.

(ii) *Photon selection*.—The genuine photons and electrons that reach to the ECAL having no reconstructed tracks are considered as photons in the Delphes neglecting the conversions of photons into electron-positron pairs. In the present version of Delphes 3.2.0, the fake rate of photons are not simulated. In our simulation, we select photons subject to cuts,

$$p_T^{\gamma} > 20\ \text{GeV}; \qquad |\eta^{\gamma}| < 2.4, \tag{4.4}$$

but excluding the η region, $1.44 < |\eta|^{\gamma} < 1.57$. The isolation of photon is ensured by measuring the sum of transverse momenta $E_T^{ac}(\gamma)$ of all particles around $\Delta R = 0.5$ along the axis of the photon and transverse momentum more than 0.5 GeV. We consider an photon is isolated if

$$E_{AC}^{T}(\gamma) < 0.2 p_T^{\gamma}. \tag{4.5}$$

(iii) *Missing transverse energy*.—In the Delphes, the missing transverse energy is estimated from the transverse component of the total energy deposited in the detector, as defined,

$$\vec{\not{E}}_T = -\sum \vec{p}_T(i), \tag{4.6}$$

where i runs over all measured collections from the detector. In the signal event $\not{E}_T$ is expected to be harder as it appears due to the comparatively heavier object $\tilde{\chi}_1^0$, where as in the SM it is mainly due to the neutrinos. Hence, $\not{E}_T$ may be a useful variable to isolate background events by a good fraction without affecting signal events too much. A cut,

$$\not{E}_T > 50\ \text{GeV}, \tag{4.7}$$

is applied in our simulation and observed that a substantial fraction ($\gtrsim$50%) of background events are rejected with a mild loss of signal events.

With a goal to separate out the signal from the background events, we investigate several kinematic variables. We notice that the p_T^{γ} are comparatively harder in the signal than the background events. This can be attributed to the fact that the photons in the signal events originate from A_1 decay, which is to some extent expected to be boosted as it is produced from heavier neutralino states. On the other hand, in the background process photons arise due to soft or hard emission accompanied with a W/Z boson and are not as boosted as in the signal events. Hence, we impose following a hard cut on the leading(γ_1) photon and a little mild on the subleading (γ_2) photon to eliminate background events,

$$p_T^{\gamma_1} > 40\ \text{GeV}; \qquad p_T^{\gamma_2} > 20\ \text{GeV}. \tag{4.8}$$

Moreover, interestingly, we observed that the distribution of $\Delta R_{\gamma_1\gamma_2}$, defined as

$$\Delta R_{\gamma_1\gamma_2} = \sqrt{(\eta_{\gamma_1} - \eta_{\gamma_2})^2 + (\phi_{\gamma_1} - \phi_{\gamma_2})^2}, \tag{4.9}$$

presents a characteristic feature for the signal events. Two photons in signal events originating from a comparatively massive A_1 are expected to be correlated without much angular separation between them, unlike the background events, where these are not directly correlated and come out with a comparatively wider angular separation. This interesting feature is clearly demonstrated in the distribution of $\Delta R_{\gamma_1\gamma_2}$, as shown in Fig. 9 (left), for both the signal and dominant backgrounds, such as $W\gamma$, $W\gamma\gamma$, $W\gamma j$. Note that

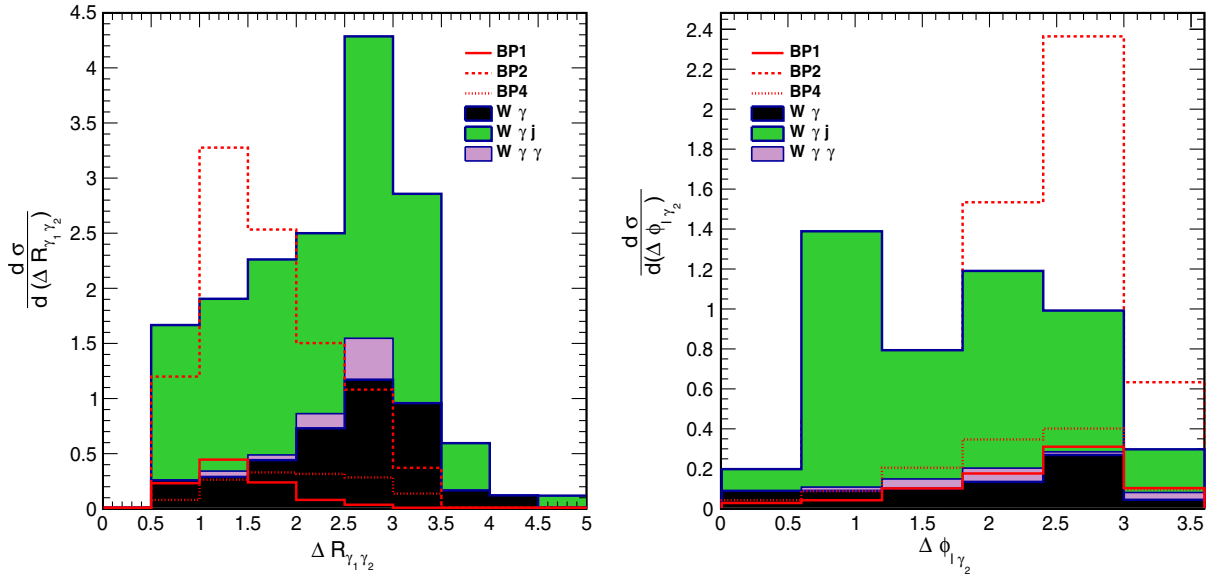

FIG. 9. $\Delta R_{\gamma_1\gamma_2}$ (left) and $\Delta\phi_{l\gamma_2}$ (right) distribution for both the signal and dominant backgrounds. These are subject to selection cuts, Eqs. (4.3), (4.7), and (4.8).

$\Delta R_{\gamma_1\gamma_2}$ distributions are subject to cuts given by Eqs. (4.3), (4.7), and (4.8). It displays a clear difference, where the signal events are distributed in the lower region of $\Delta R_{\gamma_1\gamma_2}$, whereas the background events mostly appear towards the higher side. Evidently, this characteristic feature can be exploited to improve the purity of the signal events. Optimizing the selection of $\Delta R_{\gamma_1\gamma_2}$, we require

$$\Delta R_{\gamma_1\gamma_2} \leq 2.0 \tag{4.10}$$

in our simulation and eliminate a good fraction of background events. Finally, to minimize the background contamination further, in particular due to the most dominant $W\gamma j$ process, we construct another observable, the difference in the azimuthal angle between the lepton and the subleading photon i.e. $\Delta\phi_{\ell\gamma_2}$. In Fig. 9 (right), we present the distribution of $\Delta\phi_{\ell\gamma_2}$ for both the signal and the dominant backgrounds ($W\gamma$, $W\gamma j$, $W\gamma\gamma$). This distribution clearly shows a difference in behavior of the signal events which are distributed towards the higher values of $\Delta\phi_{\ell\gamma_2}$, while the dominant $W\gamma j$ background does not show any such pattern. Hence, a selection of $\Delta\phi_{\ell\gamma_2}$ as

$$\Delta\phi_{\ell\gamma_2} > 1.5 \tag{4.11}$$

further suppresses the $W\gamma j$ background without much reduction of the signal. Also note that in this selected region of $\Delta\phi_{l\gamma_2}$, only the signal contribution corresponding to the BP1 point is large, while for the other BPs, it is more or less at the same level as backgrounds. Implementing all selection cuts together in the simulation, we achieve a reasonable signal sensitivity as discussed in the next section.

V. RESULTS

In Table II, we present the summary of our simulation for both the signal and the SM backgrounds showing the number of events remaining after applying a given set of cuts. The results are shown for the signal corresponding to six BPs as shown in Table I. The third column presents the production cross sections and N_{ev} in the fourth column indicates the number of events simulated for each processes. A k-factor 1.3 is used for the signal cross section in order to take into account NLO effects [51]. The NLO cross sections for background processes are evaluated using MadGraph aMC@NLO [64] subject to $p_T^\gamma > 10$ GeV and $|\eta^\gamma| < 2.5$ for photons, where as $p_T^j > 20$ GeV and $|\eta^j| < 5$ are also used for accompanied jets at the generating level. A requirement of two hard photons and a single lepton reduces the background contributions substantially by 3–5 orders of magnitude, whereas the signal events decrease by about an order. The $\not{E}_T > 50$ GeV selection is very effective in suppressing backgrounds, in particular the process accompanying with a Z boson in which case there is no genuine source of $\not{E}_T$. The selection of $\Delta R_{\gamma_1\gamma_2}$ appears to be very useful, as discussed above, in eliminating backgrounds by 60%–80% with a marginal reduction in signal events. Evidently, the dominant background contamination turn out to be due to the $W\gamma j$, which is about 65% of the total background contribution. Notably, the background processes associated with a Z boson are not contributing significantly, because of the requirement of a single lepton and a strong $\not{E}_T$. The signal benchmark points BP2 and BP3, comparatively with lower masses of $\tilde{\chi}_1^\pm$ and $\tilde{\chi}_2^0$ yield larger event rates, primarily due to the large production cross sections. The last columns show the cross sections normalized by the selection efficiency due to set selections for each process and parameter space.

TABLE II. Event summary for the signal and backgrounds (Bkg.) subject to a set of cuts. The last column presents the cross section after multiplying the acceptance efficiency including BRs.

	Process	σ(NLO)	N_{ev}	$N_\gamma \geq 2$	$N_l = 1$	$\not{E}_T \geq 50$	$\Delta R_{\gamma_1\gamma_2} \leq 2$	$\Delta\phi_{l\gamma_2} \geq 1.5$	$\sigma \times \epsilon$ (fb)
BP1	$\tilde{\chi}_2^0\tilde{\chi}_1^\pm$	36.4 fb	0.3L	7124	886	569	502	426	0.38
	$\tilde{\chi}_3^0\tilde{\chi}_1^\pm$	44.8 fb	0.3L	7006	879	587	519	431	0.14
BP2	$\tilde{\chi}_2^0\tilde{\chi}_1^\pm$	335 fb	0.3L	9303	1140	590	415	346	2.9
	$\tilde{\chi}_3^0\tilde{\chi}_1^\pm$	442 fb	0.3L	9593	1213	682	499	418	1.7
BP3	$\tilde{\chi}_3^0\tilde{\chi}_1^\pm$	539 fb	0.3L	5755	589	312	270	240	2.2
BP4	$\tilde{\chi}_2^0\tilde{\chi}_1^\pm$	61.1 fb	0.3L	14750	2555	1916	910	738	0.6
	$\tilde{\chi}_3^0\tilde{\chi}_1^\pm$	43.9 fb	0.3L	14827	2447	1873	935	730	0.002
BP5	$\tilde{\chi}_2^0\tilde{\chi}_1^\pm$	4.00 fb	0.3L	7798	1023	715	598	475	0.060
	$\tilde{\chi}_3^0\tilde{\chi}_1^\pm$	1.80 fb	0.3L	8292	1111	809	694	540	0.003
BP6	$\tilde{\chi}_2^0\tilde{\chi}_1^\pm$	8.80 fb	0.3L	7549	893	497	353	288	0.004
	$\tilde{\chi}_3^0\tilde{\chi}_1^\pm$	4.90 fb	0.3L	9135	1132	813	634	517	0.080
Bkg.	$W\gamma$	215 pb	30M	15002	1117	272	65	47	0.33
	$Z\ \gamma$	103 pb	30M	14792	1506	52	12	10	0.03
	$W\gamma\ j$	125 pb	2.1M	2987	282	137	49	30	1.80
	$Z\gamma\ j$	45 pb	2.1M	2531	1203	27	10	6	0.13
	$W\ \gamma\gamma$	407 fb	0.5L	6011	760	260	66	47	0.40
	$Z\ \gamma\gamma$	257 fb	0.5L	5312	233	12	7	4	0.02

In Table III, we show the sensitivity of the signal presenting the significances ($S/\sqrt{B}$) for three integrated luminosity options 100, 300 and 1000 fb^{-1}. The total background cross section is estimated to be about 2.74 fb. In this Table the second row presents the signal cross section corresponding to each BPs. The significances are quite encouraging for the lower masses ($\lesssim 400$ GeV) of $\tilde{\chi}_1^\pm, \tilde{\chi}_{2,3}^0$ and for $A_1 \sim 60$–100 GeV, even for low integrated luminosity $\mathcal{L} = 100$ fb^{-1}. However, for the higher range of masses (BP5 and BP6), the sensitivity is very poor due to tiny production cross sections. We emphasize again that, in order to obtain a detectable signal rate, the chosen parameter space happens to be a compressed scenario. In the case of the scenario represented by BP4, where $M_1 < \mu_{\rm eff}$, $\tilde{\chi}_{2,3}^0$ decays to a relative massive of A_1.

Remarkably, this signal is observable for some of the BPs corresponding to comparatively lower masses of $\tilde{\chi}_{2,3}^0$ and $\tilde{\chi}_1^\pm$ for the 300 fb^{-1} luminosity option and very robust for high luminosity option 1000 fb^{-1}. Note that the uncertainty in the background is not included, which can dilute the signal sensitivity depending on the level of uncertainty. Furthermore, it is worth mentioning here that in analogy with the SM Higgs searches, in this study also, the diphoton invariant mass is expected to show a clear peak at the mass of A_1. In Fig. 10, we show the distribution of reconstructed $m_{\gamma\gamma}$ subject to all cuts as listed in Table II. Because of the lower statistics of background events after selection, those are not shown in this figure. Perhaps, the

TABLE III. The signal cross sections after multiplying the acceptance efficiency including BRs (second row) and significance ($S/\sqrt{B}$) for three integrated luminosity options 100, 300 and 1000 fb^{-1}. The total background cross section is 2.74 fb.

Process	BP1	BP2	BP3	BP4	BP5	BP6
$\sigma \times \epsilon$ (fb)	0.52	4.6	2.2	0.6	0.063	0.084
$\mathcal{L}$ (fb^{-1})			$S/\sqrt{B}$			
100	3.1	28.1	13.3	3.5	0.40	0.50
300	5.4	48.7	23.9	6.0	0.67	0.88
1000	9.8	89.0	42.0	11.0	1.22	1.60

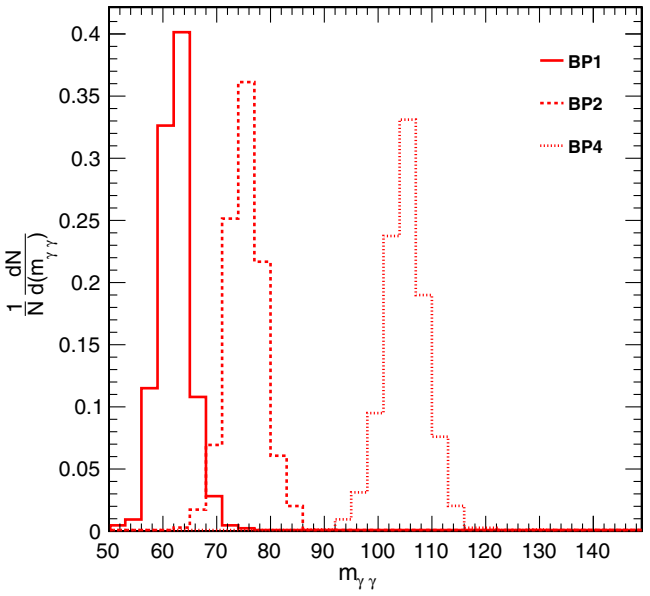

FIG. 10. Two photon invariant mass for three signal BPs normalizing to unity.

level of background contamination can be reduced further by fitting the signal peak leading an enhancement of signal sensitivity.

VI. SUMMARY

In the NMSSM, one of the non-SM-like Higgs bosons, particularly lightest pseudoscalar A_1, which is mostly singlet-like, can decay to the diphoton channel via Higgsino-like chargino loop with a substantial BR. We identify the region of the parameter space corresponding to $\mathrm{BR}(\tilde{\chi}^0_{2,3} \to \tilde{\chi}^0_1 A_1)$ and $\mathrm{BR}(A_1 \to \gamma\gamma) \geq 10\%$ or more and present the potential ranges of λ, κ along with μ_{eff}, A_λ. We investigate the sensitivity of the signal $\ell + \gamma\gamma + \not{E}_T$ producing A_1 through the chargino-neutralino associated production as shown in Eq. (1.2). The possible contamination due to the SM backgrounds is also estimated and $W\gamma j$ is found to be the dominant one, where jet fakes as a photon. Performing a detailed simulation of the signal and the background processes including detector effects using Delphes, we predict the signal sensitivity for a few benchmark points and for a given integrated luminosity options for the LHC run 2 experiments. Our simulation shows that this signal is observable marginally for 100 fb^{-1} integrated luminosity. However, for the larger integrated luminosity option, this signal is very robust and $S/\sqrt{B} \gg 5\sigma$ can be achieved for the $m_{\tilde{\chi}^0_{2,3}}$, $m_{\tilde{\chi}^\pm_1} \sim 400$ GeV and $M_{A_1} \sim 70$ GeV, whereas it severely degrades for higher masses ~600 GeV due to the heavily suppressed cross section. The reconstructed diphoton invariant mass is expected to show a clear visible narrow peak around the mass of A_1, which can be exploited to suppress backgrounds further to improve the signal sensitivity. Hence, room for more improvements of signal to background ratio exists, which is not explored in the current study. We reiterate here that two photons BR of Higgs boson is heavily suppressed in the SM and as well as in the MSSM. In this context, we emphasize again very strongly that this diphoton decay mode of A_1 can be used as a powerful tool to distinguish the NMSSM from the other SUSY models.

ACKNOWLEDGMENTS

J. K. would like to thank Bibhu P. Mahakud, Jyoti Ranjan Beuria and Michael Paraskevas for useful discussions. The authors are also thankful to Saurabh Nioygi for participating in this project at the beginning.

[1] G. Aad *et al.* (ATLAS Collaboration), Observation of a new particle in the search for the standard model Higgs boson with the ATLAS detector at the LHC, Phys. Lett. B **716**, 1 (2012).
[2] S. Chatrchyan *et al.* (CMS Collaboration), Observation of a new boson at a mass of 125 GeV with the CMS experiment at the LHC, Phys. Lett. B **716**, 30 (2012).
[3] L. J. Hall, D. Pinner, and J. T. Ruderman, A natural SUSY Higgs near 126 GeV, J. High Energy Phys. 04 (2012) 131.
[4] A. Arbey, M. Battaglia, A. Djouadi, F. Mahmoudi, and J. Quevillon, Implications of a 125 GeV Higgs for supersymmetric models, Phys. Lett. B **708**, 162 (2012).
[5] J. E. Kim and H. P. Nilles, The mu problem and the strong CP problem, Phys. Lett. **B138**, 150 (1984).
[6] P. Fayet, Supergauge invariant extension of the Higgs mechanism and a model for the electron and its neutrino, Nucl. Phys. **B90**, 104 (1975).
[7] J. R. Ellis, J. F. Gunion, H. E. Haber, L. Roszkowski, and F. Zwirner, Higgs bosons in a nonminimal supersymmetric model, Phys. Rev. D **39**, 844 (1989).
[8] M. Drees, Supersymmetric models with extended Higgs sector, Int. J. Mod. Phys. A **04**, 3635 (1989).
[9] U. Ellwanger, C. Hugonie, and A. M. Teixeira, The next-to-minimal supersymmetric standard model, Phys. Rep. **496**, 1 (2010).
[10] D. J. Miller, R. Nevzorov, and P. M. Zerwas, The Higgs sector of the next-to-minimal supersymmetric standard model, Nucl. Phys. **B681**, 3 (2004).
[11] Z. Kang, J. Li, and T. Li, On naturalness of the MSSM and NMSSM, J. High Energy Phys. 11 (2012) 024.
[12] J. Cao, F. Ding, C. Han, J. M. Yang, and J. Zhu, A light Higgs scalar in the NMSSM confronted with the latest LHC Higgs data, J. High Energy Phys. 11 (2013) 018.
[13] D. Albornoz Vasquez, G. Belanger, C. Boehm, J. Da Silva, P. Richardson, and C. Wymant, The 125 GeV Higgs in the NMSSM in light of LHC results and astrophysics constraints, Phys. Rev. D **86**, 035023 (2012).
[14] S. F. King, M. Muhlleitner, and R. Nevzorov, NMSSM Higgs benchmarks near 125 GeV, Nucl. Phys. **B860**, 207 (2012).
[15] S. Heinemeyer, O. Stal, and G. Weiglein, Interpreting the LHC Higgs search results in the MSSM, Phys. Lett. B **710**, 201 (2012).
[16] F. Domingo and G. Weiglein, NMSSM interpretations of the observed Higgs signal, J. High Energy Phys. 04 (2016) 095.
[17] A. Djouadi *et al.*, Benchmark scenarios for the NMSSM, J. High Energy Phys. 07 (2008) 002.
[18] S. F. King, M. Mhlleitner, R. Nevzorov, and K. Walz, Natural NMSSM Higgs bosons, Nucl. Phys. **B870**, 323 (2013).
[19] N. D. Christensen, T. Han, Z. Liu, and S. Su, Low-mass Higgs bosons in the NMSSM and their LHC implications, J. High Energy Phys. 08 (2013) 019.
[20] J. Kumar and M. Paraskevas, Distinguishing between MSSM and NMSSM through $\Delta F = 2$ processes, J. High Energy Phys. 10 (2016) 134.

[21] M. Guchait and J. Kumar, Light Higgs bosons in NMSSM at the LHC, Int. J. Mod. Phys. A **31**, 1650069 (2016).
[22] J. F. Gunion, Y. Jiang, and S. Kraml, The constrained NMSSM and Higgs near 125 GeV, Phys. Lett. B **710**, 454 (2012).
[23] U. Ellwanger and C. Hugonie, Higgs bosons near 125 GeV in the NMSSM with constraints at the GUT scale, Adv. High Energy Phys. **2012**, 625389 (2012).
[24] M. Badziak, M. Olechowski, and S. Pokorski, New regions in the NMSSM with a 125 GeV Higgs, J. High Energy Phys. 06 (2013) 043.
[25] S. Chatrchyan *et al.* (CMS Collaboration), Search for a Light Pseudoscalar Higgs Boson in the Dimuon Decay Channel in pp Collisions at $\sqrt{s} = 7$ TeV, Phys. Rev. Lett. **109**, 121801 (2012).
[26] V. Khachatryan *et al.* (CMS Collaboration), Search for a low-mass pseudoscalar Higgs boson produced in association with a $b\bar{b}$ pair in pp collisions at $\sqrt{s} = 8$ TeV, Phys. Lett. B **758**, 296 (2016).
[27] G. Aad *et al.* (ATLAS Collaboration), Search for Higgs bosons decaying to aa in the $\mu\mu\tau\tau$ final state in pp collisions at $\sqrt{s} = 8$ TeV with the ATLAS experiment, Phys. Rev. D **92**, 052002 (2015).
[28] G. Aad *et al.* (ATLAS Collaboration), Search for new phenomena in events with at least three photons collected in pp collisions at $\sqrt{s} = 8$ TeV with the ATLAS detector, Eur. Phys. J. C **76**, 210 (2016).
[29] U. Ellwanger, J. F. Gunion, C. Hugonie, and S. Moretti, NMSSM Higgs discovery at the LHC, in physics at TeV colliders, *Proceedings, Workshop, Les Houches, France, 2003* (2004), arXiv:hep-ph/0401228.
[30] U. Ellwanger, Higgs bosons in the next-to-minimal supersymmetric standard model at the LHC, Eur. Phys. J. C **71**, 1782 (2011).
[31] S. F. King, M. Mhlleitner, R. Nevzorov, and K. Walz, Discovery prospects for NMSSM Higgs bosons at the high-energy large hadron collider, Phys. Rev. D **90**, 095014 (2014).
[32] F. Mahmoudi, J. Rathsman, O. Stal, and L. Zeune, Light Higgs bosons in phenomenological NMSSM, Eur. Phys. J. C **71**, 1608 (2011).
[33] N.-E. Bomark, S. Moretti, S. Munir, and L. Roszkowski, A light NMSSM pseudoscalar Higgs boson at the LHC redux, J. High Energy Phys. 02 (2015) 044.
[34] A. Belyaev, S. Hesselbach, S. Lehti, S. Moretti, A. Nikitenko, and C. H. Shepherd-Themistocleous, The scope of the 4 tau channel in Higgs-strahlung and vector boson fusion for the NMSSM no-lose theorem at the LHC, arXiv:0805.3505.
[35] A. Belyaev, J. Pivarski, A. Safonov, S. Senkin, and A. Tatarinov, LHC discovery potential of the lightest NMSSM Higgs in the $h1 \to a\ a1 \to 4$ muons channel, Phys. Rev. D **81**, 075021 (2010).
[36] M. M. Almarashi and S. Moretti, Muon signals of very light CP-odd Higgs states of the NMSSM at the LHC, Phys. Rev. D **83**, 035023 (2011).
[37] D. G. Cerdeno, P. Ghosh, and C. B. Park, Probing the two light Higgs scenario in the NMSSM with a low-mass pseudoscalar, J. High Energy Phys. 06 (2013) 031.
[38] D. Curtin, R. Essig, and Y.-M. Zhong, Uncovering light scalars with exotic Higgs decays to $b\bar{b}\mu^+\mu^-$, J. High Energy Phys. 06 (2015) 025.
[39] N.-E. Bomark, S. Moretti, and L. Roszkowski, Detection prospects of light NMSSM Higgs pseudoscalar via cascades of heavier scalars from vector boson fusion and Higgs-strahlung, J. Phys. G **43**, 105003 (2016).
[40] A. Arhrib, K. Cheung, T.-J. Hou, and K.-W. Song, Associated production of a light pseudoscalar Higgs boson with a chargino pair in the NMSSM, J. High Energy Phys. 03 (2007) 073.
[41] R. Dermisek and J. F. Gunion, The NMSSM solution to the fine-tuning problem, precision electroweak constraints and the Largest LEP Higgs event excess, Phys. Rev. D **76**, 095006 (2007).
[42] J. E. Kim, H. P. Nilles, and M.-S. Seo, Singlet superfield extension of the minimal supersymmetric standard model with Peccei-Quinn symmetry and a light pseudoscalar Higgs boson at the LHC, Mod. Phys. Lett. A **27**, 1250166 (2012).
[43] U. Ellwanger and M. Rodriguez-Vazquez, Discovery prospects of a light scalar in the NMSSM, J. High Energy Phys. 02 (2016) 096.
[44] S. Moretti and S. Munir, Diphoton Higgs signals at the LHC in the next-to-minimal supersymmetric standard model, Eur. Phys. J. C **47**, 791 (2006).
[45] D. Ghosh, M. Guchait, and D. Sengupta, Higgs signal in chargino-neutralino production at the LHC, Eur. Phys. J. C **72**, 2141 (2012).
[46] D. G. Cerdeo, P. Ghosh, C. B. Park, and M. Peir, Collider signatures of a light NMSSM pseudoscalar in neutralino decays in the light of LHC results, J. High Energy Phys. 02 (2014) 048.
[47] M. Guchait, Exact solution of the neutralino mass matrix, Z. Phys. C **57**, 157 (1993); Erratum, Z. Phys. C **61**, 178(E) (1994).
[48] S. Y. Choi, J. Kalinowski, G. A. Moortgat-Pick, and P. M. Zerwas, Analysis of the neutralino system in supersymmetric theories, Eur. Phys. J. C **22**, 563 (2001); Erratum, Eur. Phys. J. C **23**, 769 (2002).
[49] P. N. Pandita, Neutralino mass matrix in the nonminimal supersymmetric standard model, Z. Phys. C **63**, 659 (1994).
[50] S. Y. Choi, D. J. Miller, and P. M. Zerwas, The neutralino sector of the next-to-minimal supersymmetric standard model, Nucl. Phys. **B711**, 83 (2005).
[51] W. Beenakker, M. Klasen, M. Kramer, T. Plehn, M. Spira, and P. M. Zerwas, The Production of Charginos/Neutralinos and Sleptons at Hadron Colliders, Phys. Rev. Lett. **83**, 3780 (1999); Erratum, Phys. Rev. Lett. **100**, 029901(E) (2008).
[52] H.-L. Lai, M. Guzzi, J. Huston, Z. Li, P. M. Nadolsky, J. Pumplin, and C. P. Yuan, New parton distributions for collider physics, Phys. Rev. D **82**, 074024 (2010).
[53] W. Beenakker, R. Hopker, and M. Spira, PROSPINO: A program for the production of supersymmetric particles in next-to-leading order QCD, arXiv:hep-ph/9611232.
[54] U. Ellwanger, J. F. Gunion, and C. Hugonie, NMHDECAY: A Fortran code for the Higgs masses, couplings and decay widths in the NMSSM, J. High Energy Phys. 02 (2005) 066.
[55] S. Munir, L. Roszkowski, and S. Trojanowski, Simultaneous enhancement in $\gamma\gamma$, $b\bar{b}$ and $\tau^+\tau^-$ rates in the NMSSM

with nearly degenerate scalar and pseudoscalar Higgs bosons, Phys. Rev. D **88**, 055017 (2013).
[56] M. Spira, A. Djouadi, D. Graudenz, and P. M. Zerwas, Higgs boson production at the LHC, Nucl. Phys. **B453**, 17 (1995).
[57] M. Spira, QCD effects in Higgs physics, Fortschr. Phys. **46**, 203 (1998).
[58] G. Aad *et al.* (ATLAS and CMS Collaborations), Measurements of the Higgs boson production and decay rates and constraints on its couplings from a combined ATLAS and CMS analysis of the LHC pp collision data at $\sqrt{s} = 7$ and 8 TeV, J. High Energy Phys. 08 (2016) 045.
[59] T. Sjostrand, S. Mrenna, and P. Z. Skands, PYTHIA 6.4 Physics and Manual, J. High Energy Phys. 05 (2006) 026.
[60] P. Z. Skands *et al.*, SUSY Les Houches accord: Interfacing SUSY spectrum calculators, decay packages, and event generators, J. High Energy Phys. 07 (2004) 036.
[61] G. Aad *et al.* (ATLAS Collaboration), Search for direct pair production of a chargino and a neutralino decaying to the 125 GeV Higgs boson in $\sqrt{s} = 8$ TeV pp collisions with the ATLAS detector, Eur. Phys. J. C **75**, 208 (2015).
[62] P. L. L. Garren, *StdHep User Manual*.
[63] J. de Favereau, C. Delaere, P. Demin, A. Giammanco, V. Lematre, A. Mertens, and M. Selvaggi (DELPHES 3 Collaboration), DELPHES 3, A modular framework for fast simulation of a generic collider experiment, J. High Energy Phys. 02 (2014) 057.
[64] J. Alwall, R. Frederix, S. Frixione, V. Hirschi, F. Maltoni, O. Mattelaer, H. S. Shao, T. Stelzer, P. Torrielli, and M. Zaro, The automated computation of tree-level and next-to-leading order differential cross sections, and their matching to parton shower simulations, J. High Energy Phys. 07 (2014) 079.